(Zn,Cd)Se/ZnSe quantum-well lasers: Excitonic gain in an inhomogeneously broadened quasi-two-dimensional system

J. Ding, M. Hagerott, T. Ishihara,* H. Jeon, and A. V. Nurmikko
Division of Engineering and Department of Physics, Brown University, Providence, Rhode Island 02912
(Received 23 June 1992; revised manuscript received 30 December 1992)

Optical properties of a strongly excitonic quasi-two-dimensional system in a wide-band-gap II-VI semiconductor heterostructure are investigated in terms of the relationship between absorption and stimulated emission. In particular, the optical gain in (Zn,Cd)Se/ZnSe quantum-well lasers is demonstrated to be of excitonic nature over a wide range of temperatures, and to occur at electron-hole pair densities below the exciton-electron hole plasma transition. Both steady-state and transient (picosecond and femtosecond) spectroscopic techniques have been applied to detail exciton kinetics within the $n=1$ heavy-hole exciton resonance. A phenomenological model of optical gain is proposed; originating from an inhomogeneously broadened exciton resonance and including the effects of exciton-phonon interaction.

I. INTRODUCTION

A major recent event in the field of II-VI compound semiconductors has been the proof-of-concept demonstration of a blue-green diode laser.[1,2] Important ingredients to this success include advances in p-type doping of ZnSe,[3] and improvement in both material quality and physical understanding of quantum wells (QW's) and related heterostructures. In particular, the first diode lasers incorporated the (Zn,Cd)Se/ZnSe QW as the active medium, suggested by earlier studies using optical pumping.[4] More recently, diode laser operation at shorter wavelengths in pseudomorphic (Zn,Cd)Se/Zn(S,Se) [Ref. 5(a)] and (Zn,Cd)Se/(Zn,Mg)Se [Ref. 5(b)] QW heterostructures has also been achieved, with the latter extending the wavelength deeper into the blue. To date, pulsed operation up to room temperature and continuous-wave (cw) operation at 77 K have been demonstrated by both the 3M group and the Brown-Purdue team in these ZnSe-based QW lasers. Following this early success, microscopic understanding of the gain mechanism of these lasers is now an important issue for their further design in order to achieve room-temperature continuous-wave (cw) operation. (Other major challenges include further improvement in p doping and solving the Ohmic-contact problem.) The standard model which for three decades has been used to model the population inversion and gain in III-V and other semiconductor lasers, including QW lasers, is based on the degenerate-electron-hole-plasma (EHP) picture. For the type-I (Zn,Cd)Se/ZnSe quantum-well system, however, it has been demonstrated recently that the quasi-two-dimensional confinement of electron-hole pairs leads to an enhancement of the exciton oscillator strength as well as its binding energy E_x, such that the latter exceeds the longitudinal-optical (LO)-phonon energy $\hbar\omega_{\mathrm{LO}}$, that is, $E_x \approx 40$ meV $> \hbar\omega_{\mathrm{LO}} = 30.5$ meV.[6] As one consequence, strong distinct exciton absorption features can be seen well above room temperature. The questions then arise as to whether exciton effects might have fundamental and practical consequences in recombination processes, especially in laser structures.

In this paper, we present a detailed study of the multiple (Zn,Cd)Se/ZnSe quantum-well system as a gain medium using optical pumping techniques, and focus on the role of the $n=1$ heavy-hole (HH) exciton resonance and its contribution to the stimulated emission. The paper is organized as follows. In Sec. II, we review some of the basic quantum-well physics of the (Zn,Cd)Se/ZnSe system. Consistent with type-I electron-hole confinement and enhanced excitonic effects in a wide-gap II-VI system, we show that a large reduction of the homogeneous broadening and a large enhancement of oscillator strength occurs at the $n=1$ HH exciton resonance. In Sec. II, we present the experimental evidence to argue that excitons do indeed play a central role in the formation of gain in the (Zn,Cd)Se/ZnSe QW's, which have emerged as the prime candidates for diode lasers in the blue-green portion of the visible spectrum. By employing both steady-state and picosecond spectroscopy, we show that the origin of gain and laser action in (Zn,Cd)Se/ZnSe quantum wells in the blue-green wavelengths is predominantly of excitonic nature at least to about 220 K, and appears to be important at room temperature as well. Among other experimental observations, we find that stimulated emission occurs when photoexcitation takes place resonantly into the $n=1$ HH exciton absorption line. In Sec. IV, we draw a phenomenological model of the physical processes involved in the formation of optical gain in which the inhomogeneously broadened character of the exciton resonance is found to provide us with an effective multilevel system. We argue, supported by the experimental measurements, that at the pair densities at which such an exciton system can provide gain, a transition to an EHP has not yet taken place. This proposition does not exclude the possibility that a degenerate EHP is responsible for laser emission in practical circumstances, where much higher densities are called for

(to overcome losses). In Sec. V, the results of picosecond pump-probe measurements are presented. In addition to demonstrating directly that the optical gain coexists with the exciton absorption feature, the results also provide us with better understanding of the exciton dynamics in terms of energy relaxation and phase-space filling within the inhomogeneous line. Section VI includes, among other things, the femtosecond pump-probe experimental results. The reconstructed gain/absorption spectra at certain times after photoexcitation provide the ultimate proof that the well-defined $n=1$ HH exciton resonance (absorption peak) provides optical gain at its low-energy side. The advantages of using the picosecond and femtosecond pump-probe techniques on our inhomogeneously broadened exciton system are also compared and discussed. In Sec. VII, we comment briefly on the relevance of this work to the blue-green diode lasers. We summarize the paper in Sec. VIII.

II. THE (Zn,Cd)Se/ZnSe QUANTUM WELL

The (Zn,Cd)Se/ZnSe quantum-well structures which are the subject of this study were grown by molecular-beam epitaxy (MBE) on (001) GaAs substrates (the growth direction is defined here as the z direction), atop which a buffer layer on ZnSe of 0.5–1 μm thickness was first deposited. The quantum-well sections were followed by a 0.2-μm cap layer of ZnSe. The initial description of the epitaxial growth of (Zn,Cd)Se has been reported elsewhere.[7] During this work, we studied dozens of different (ZnCd)Se/ZnSe quantum-well structures (both single or multiple wells), grown at both the University of Notre Dame and Purdue University, with very similar results. The two particular multiple-quantum-well structures we will focus on in this paper consist of six undoped $Zn_{0.76}Cd_{0.24}Se$ wells of thickness $L_w=90$ and 30 Å, separated by 500-Å undoped ZnSe barrier layers. The ZnSe cap and buffer layers with the QW segment sandwiched in between also form an optical waveguide for light that propagates in the layer plane,[8] which is another requirement for a semiconductor laser device. The recent diode laser structures[1,2,5] differ chiefly by the presence of thicker buffer and cap layers, doped to form the pn-junction injector structure.

We now review some of the relevant basic features of the (Zn,Cd)Se/ZnSe QW based on optical-absorption spectroscopy. A more detailed description of these results can be found in the work by Pelekanos *et al.*[6(b)]

The bottom panel of Fig. 1 shows the absorption spectra of the 90-Å QW sample at different temperatures (the GaAs substrate was chemically removed for the transmission measurement). The dominant $n=1$ HH exciton absorption features are well defined from 10 to 300 K. This is in strong contrast with bulk ZnSe, where the large exciton–LO-phonon interaction renders the exciton states invisible well below room temperature. The peak absorption coefficient corresponds to $\alpha=1.1\times10^5$ cm^{-1} at 10 K if the effective optical thickness is taken to be 6×90 Å$=540$ Å. The full width at half maximum (FWHM) of the absorption profile is measured to be 9 meV at 10 K. If we assume a Gaussian line shape for the

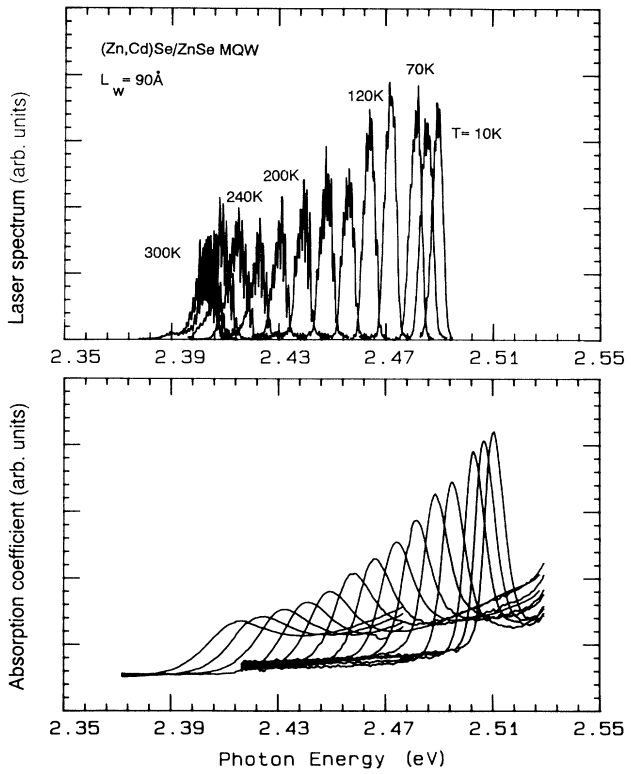

FIG. 1. Pulsed laser emission spectrum (top panel) and absorption spectrum of the unexcited sample (bottom panel) of a 6×90 Å, (Zn,Cd)Se/ZnSe MQW structure at 10, 50, 70, 100, 120, 140, 160, 180, 200, 220, 240, 260, 280, and 300 K, respectively.

1s exciton resonance, the oscillator strength for the exciton [proportional to $L_w\int\alpha\,dE$ (Ref. 9)] is calculated to be approximately 2×10^{-2}. During the course of this work, we studied quantum-well structures of various well widths ranging from 30 to 90 Å, and results consistent with Fig. 1 (bottom panel) are obtained in these quasi-2D (two-dimensional) conditions. The low-temperature exciton absorption linewidths can be attributed to the alloy composition and well thickness fluctuations (inhomogeneous broadening). With increasing temperature, the linewidth increases because of the exciton–LO-phonon interaction (adding to the homogeneous broadening). The LO-phonon-induced exciton lifetime shortening (dissociation into e-h continuum states) gives a dominant contribution to the homogeneous broadening of the resonance at higher temperatures. Magnetoexcitation absorption measurements have also been performed on this quantum-well structure, the details of which can be found in the work by Pelekanos *et al.*[6(b)] The binding energy of the quasi-2D excitons in this QW system has been determined to range from 35 to 41 meV, hence exceeding the LO-phonon energy in ZnSe (approximately 31 meV). This result manifests itself in a large reduction in the LO-phonon–exciton coupling. In bulk (3D) ZnSe, the direct dissociation of excitons into its continuum states is energetically allowed because the binding energy of the exciton [$E_x\approx17$ meV (Ref. 10)] is less than $\hbar\omega_{LO}$ (30.5

meV), whereas in our quantum-well structures, the quasi-2D confinement in both conduction and valence bands (see below) enlarges the exciton binding energy so that such processes are energetically forbidden. This is a key factor in explaining room-temperature exciton absorption, in addition to the 2D enhancement of the oscillator strength. We would like to emphasize that such a situation cannot occur in, e.g., $Ga_{1-x}Al_xAs/GaAs$ QW's, where the quantum confinement increases the exciton binding energy from the bulk value of 4 meV to about 10 meV,[11] a value still well below the LO-phonon energy of 36 meV. As a result, the room-temperature absorption features of $Ga_{1-x}Al_xAs/GaAs$ QW structures are mostly due to the enhancement of the oscillator strength, and the exciton resonance is dominated by homogeneous broadening in high-quality material.

The experimentally determined temperature dependence of the exciton absorption linewidth (crosses) for our sample is presented in Fig. 2, where a fit is described by the following equation:[11]

$$\Gamma=\Gamma_0+\Gamma_1(T)+\frac{\Gamma_{\mathrm{LO}}}{(e^{\hbar\omega_{\mathrm{LO}}/kT}-1)}\ , \tag{1}$$

where Γ_0 is the inhomogeneous broadening, $\Gamma_1(T)$ is the homogeneous broadening contribution from the acoustic-phonon exciton scattering, and Γ_{LO} characterizes the exciton–LO-phonon coupling strength. Using the approach by Lee, Koteles, and Vassell,[12] we can estimate that the linewidth broadening contribution from the acoustic phonons is much less important than that from the LO phonons. The best fit gives the value for Γ_{LO} of approximately 36 meV. The linewidth calculation using the equation above and a Γ_{LO} value of 60 meV, a lower limit for bulk ZnSe, is also plotted in the graph. The reduction in the value of Γ_{LO} indicates the reduction in the exciton dissociation rate by LO phonons and the absorption linewidth broadening, i.e., reduced homogeneous broadening of the exciton resonance.

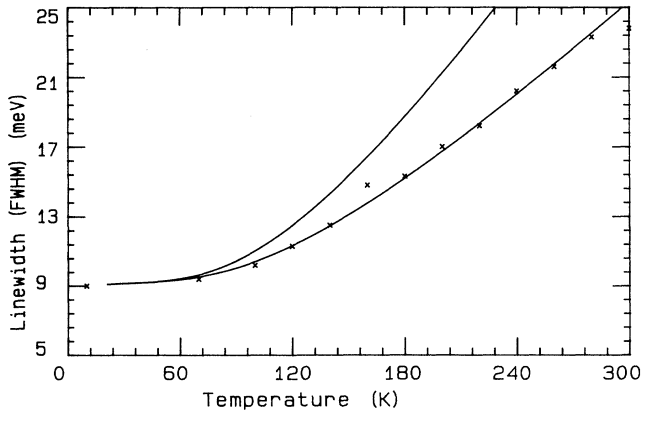

FIG. 2. The linewidth of the exciton absorption of the 6×90 Å (Zn,Cd)Se/ZnSe quantum-well structure at different temperatures (crosses). The solid line is a fit using Eq. (1); the calculated linewidth using $\Gamma_{\mathrm{LO}}=60$ meV for bulk ZnSe is also included.

We also briefly comment on the issue of band offsets and the electronic confinement in the conduction and valence bands in our QW's. There is a rather large lattice mismatch between the ZnSe barrier layers and (Zn,Cd)Se QW layers for a 24% Cd concentration ($\Delta a/a \approx 1.7\%$). Under the assumption of pseudomorphic growth, the strain is accommodated elastically in the (Zn,Cd)Se QW layers. Our calculations published earlier,[6(b)] based on the optical transition energies and including effects of strain by using Van de Walle's approach,[13] indicate that the valence-band offset for the HH band is about 55 meV (about 30 meV without strain), and that of the conduction band is 190 meV for the particular sample discussed here. The strain-enhanced HH valence-band offset thus aids in realizing a quasi-2D exciton system. We note that in the more recent (Zn,Cd)Se/Zn(S,Se) QW system, the valence-band offset is further increased due to the introduction of sulfur in the barrier layers.

III. OPTICAL PUMPING OF QW LASERS

A. Experimental configuration and observation of laser emission

The experimental geometry in our optical pumping experiments of QW lasers is shown in Fig. 3. The (Zn,Cd)Se/ZnSe QW samples were cleaved to form resonators ranging from 60 μm to 1 mm in length, with uncoated or coated facets, and were excited perpendicular to the quantum-well layer plane. Edge emission through a cleaved facet was directed to a distant spectrometer without the need of collection optics, when investigating the onset of lasing (by detecting a laser's far-field emission) and the subsequent behavior as a function of the excitation level and the dependence on photon energy. Collection optics were added when studying the evolution of the edge emission from luminescence to lasing over a wide dynamical range. Three modes of photoexcitation were employed: (i) a pulsed dye laser tunable throughout the blue-green wavelength region (5-ns pulsewidth, 200-Hz repetition rate) excited by an excimer laser; (ii) a tunable synchronously pumped picosecond blue-green dye

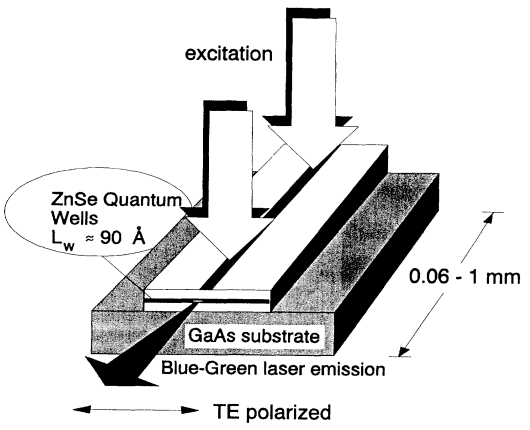

FIG. 3. The schematic diagram of the experimental arrangement for the optical pumping of the QW lasers.

laser pumped by the third-harmonic generation (THG) of the Nd:YAG (yttrium aluminum garnet) laser; (iii) the second-harmonic generation of a mode-locked femtosecond Ti:sapphire laser operating in the long-wavelength range. The first method provides steady-state excitation and the latter methods allowed us to make dynamical measurements and to study possible gain switching for an individual pulse event on a time scale shorter than the electron-hole pair lifetime. The time resolution in the detection was obtained by using a streak camera to register the dynamics of the laser output. The onset of laser emission could be observed visually from a sudden increase in the brightness of the edge emission, in the form of a highly asymmetric angular far-field emission pattern which diverged strongly in the z direction (indicating effective waveguide confinement), while remaining well collimated in the perpendicular direction. The stimulated emission was strongly TE polarized, as expected from the optical selection rules for the symmetric quantum-well $n=1$ interband transition. Spectra from a quantum-well laser of 200-μm cavity length at different temperatures and under the nanosecond dye laser excitation at photon energies above the ZnSe band gap are shown in the top panel of Fig. 1 to highlight the spectral correlation with the exciton absorption spectra in an unexcited sample. Room-temperature lasing was obtained at a threshold intensity of excitation of approximately 100 kW/cm^2 for such a cavity length, whereas at 10 K the threshold is about 10 kW/cm^2. The room-temperature threshold intensity decreased to about 30 kW/cm^2 for the same quantum-well structure with a 600-μm cavity length, hence we conclude that reflection at the uncoated end facets presents the dominant loss mechanism (the reflection coefficient was measured to be 21% per facet). From such observations, we can further estimate that the threshold gain coefficient for our lasers is on the order of 80 cm^{-1} for a laser of 200-μm cavity length. We note that the typical cavity lengths in the recent blue-green diode lasers have been longer, on the order of 1 mm. Pumped by an UV argon-ion laser, cw operation was realized up to 100 K, where a duty cycle of 10^{-2} was employed to reduce the lattice heating for device lifetime reasons.[4(c)]

B. Laser spectra and their correlation with absorption

The spectral range for the laser emission in Fig. 1 occurs within the $n=1$ HH exciton region, as defined by the corresponding absorption spectra. Comparison between the measured peak positions of the stimulated emission and the absorption from 10 to 300 K shows a largely temperature-independent correlation between the stimulated emission and absorption, namely, that the former is related to the latter by a spectral redshift on the order of 20 meV. This general behavior was verified by similar observations of many different QW structures where in each case a well-defined room-temperature exciton was observed in absorption. Closer examination of data such as that in Fig. 1 shows that the stimulated emission spectra in fact overlap with the low-energy tail of the corresponding absorption spectra at each given

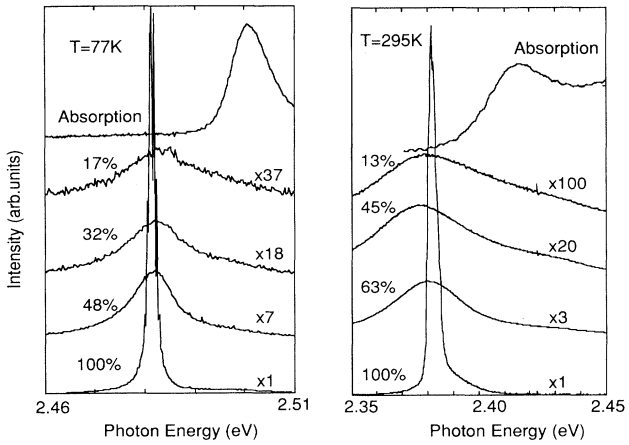

FIG. 4. The evolution of the 6×90 Å MQW laser emission from the spontaneous emission spectrum at $T=77$ and 295 K for laser devices of 200 and 780 μm, respectively. The $n=1$ HH exciton absorption spectra are also shown for reference. The excitation level is indicated by the percentage of the maximum used in the experiment, which was slightly above the laser threshold.

temperature. The large redshift of the lasing spectral position with respect to the band gap in the QW ($\approx$20 meV+exciton binding energy $\approx$60 meV in total) is not compatible with estimates of the magnitude of band-gap renormalization if the emission emanated from a free EHP, given the experimentally determined electron-hole pair density (see below).

Further evidence of the possible excitonic nature of lasing emission in the (Zn,Cd)Se QW system is shown in Fig. 4, which demonstrates how the stimulated emission emerges directly from spontaneous edge emission spectra in the $n=1$ HH exciton region at $T=77$ and 295 K (shown here with spectral resolution sufficient to display the longitudinal-mode structure of the laser). The percentages in Fig. 4 refer to the maximum excitation intensity (100%) of the nanosecond pulsed dye laser with a photon energy of 2.8 eV. We chose two laser devices of 200- and 780-μm cavity lengths, so that they have approximately the same threshold excitation intensity at 77 and 295 K, respectively. The exciton absorption resonance of the unexcited sample is reproduced for spectral reference. The rather large redshift between the photoluminescence under low excitation and the absorption is simply due to the reabsorption effect in the edge emission geometry. We have performed these experiments at excitation levels beginning as low as four orders of magnitude below the laser threshold intensity to demonstrate the lack of any substantial spectral shifts, which are usually used as indicators of the emergence of the EHP, given the density dependence of the band-gap renormalization (see, however, the discussion of cavity length dependence at the end of Sec. V).

C. Laser emission under resonant excitation

In order to isolate explicitly the possible excitonic component in the stimulated emission, we also studied the

case of laser operation under *direct resonant excitation* into the $n=1$ HH exciton ground state ($1s$). Well-defined laser emission was readily obtained over a wide range of temperatures up to 220 K (eventually limited by the available pump-laser power and wavelength tuning range of our dye laser). Here we focus on the behavior at $T=10$ K, since the initial generation of a cold gas of excitons is unambiguous in this case. Issues relevant to higher temperatures will be discussed below in the analysis of our data and model. Figure 5 shows an example of the resonant pumping data, taken here under mode-locked ps-pulsed excitation of constant intensity. This mode of excitation is useful because it allows a precise determination of the initial photon density deposited into each quantum well (from the known absorption coefficient and an accurate knowledge of the energy of each individual excitation pulse). Some of the pump-laser light was intentionally scattered into the spectrometer to provide a spectral reference as displayed in the figure, which also includes the $n=1$ HH exciton absorption resonance for the unexcited sample (top trace). At near threshold excitation level (a form of excitation spectroscopy for *stimulated* emission), Fig. 5 demonstrates vividly that laser emission is optimized when the incident photon energy is set at the peak of the HH exciton absorption. This is due simply to the optimal coupling of the photons into the exciton resonance, which is also direct evidence of the preservation of the exciton resonance during the stimulated emission event. The maximum electron-hole pair density possible in the experiment represented by Fig. 5 can be calculated to be 7×10^{11} cm^{-2}, given the incident excitation energy flux of 0.9 $\mu J/cm^2$ (and taking into account the reflections from the surfaces of the sample and optical components in addition to the absorption by the QW). Such a pair density is much lower than the exciton phase-space filling density (see below) in our system, which is estimated to be $1/\pi a_B^2 \approx 5.1\times10^{12}$ cm^{-2}, and the experimental fact that laser emission is obtained under direct resonance excitation of the $n=1$ HH exciton adds considerable direct support to the idea that excitons are directly responsible for the lasing.

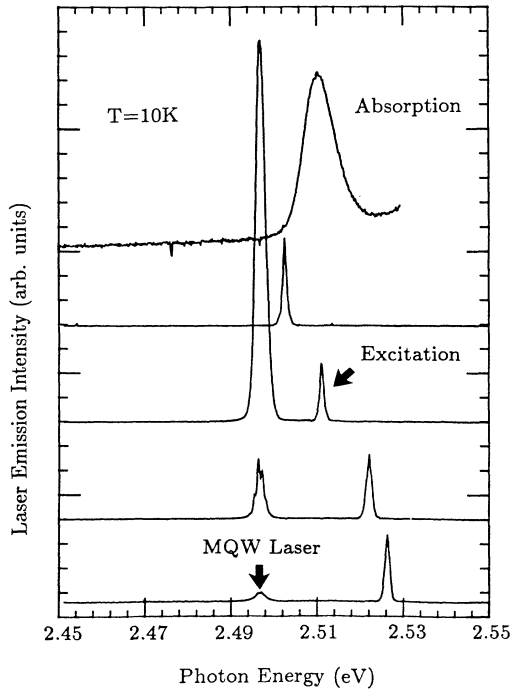

FIG. 5. The resonant pumping of the 6×90 Å (Zn,Cd)Se/ZnSe MQW laser at $T=10$ K, with the top trace showing the $n=1$ HH exciton absorption resonance of the unexcited sample. The pump photon energy is obtained by intentionally scattering this source into the spectrometer.

IV. EXCITONIC GAIN—A PHENOMENOLOGICAL MODEL FOR AN INHOMOGENEOUSLY BROADENED SYSTEM

The possibility of excitonic gain and stimulated emission in wide-gap II-VI semiconductors was first suggested by Hvam in connection with his experiments on bulk CdS and ZnO,[14] followed by comparable work in other bulk II-VI materials,[15–18] recently revisited in bulk ZnSe.[19] These experiments on bulk samples were generally performed at liquid-helium temperatures and under very high optical excitations. The lack of clear exciton absorption spectra (even at low temperatures) made the argument less convincing. In modeling of the previous work, the electron-exciton exciton-exciton or exciton–optical-phonon scattering processes[14–17,19] were argued to be essential for a gain mechanism. Under the assumption of both energy and momentum-conservation holding, these models predicted gain at photon energies distinctly below and separate from the exciton absorption edge. Our experimental observations cannot be interpreted using these models. For instance, in the resonant pumping experiment presented in Sec. III, where the only species created in the system are excitons, we find that the stimulated emission wavelength is wholly *independent* of the variations in the pump-photon energy across the exciton absorption spectrum (see Fig. 5), indicating that a quasiequilibrium among the excitons is quickly reached (on a picosecond time scale, as shown in both Secs. V and VI). That is, given the inhomogeneous exciton resonance, real exciton population relaxation effects are the most direct cause for providing exciton distributions from which gain can be extracted. The spectral position of the laser emission is 14 meV below the peak of the exciton absorption in Fig. 5 (though there is some variation in this value in general, depending on the resonator length, i.e., the threshold gain). Given the exciton binding energy of 35–40 meV, energetic considerations alone will exclude the earlier exciton-exciton scattering picture,[14–17,19] in which both energy and momentum are assumed to be conserved. We have also performed separate experiments to study exciton–LO-phonon coupling through the Raman-scattering spectrum on this QW structure, as shown in Fig. 6. The excitation photon energy is tuned around the exciton absorption peak (2.511 eV). The photon energy of the Raman scattering (denoted by the arrow in Fig. 6) is one LO-phonon energy ($\hbar\omega_{LO}$) below the excitation photon energy. Such experimental data confirms the value of approximately 30 meV

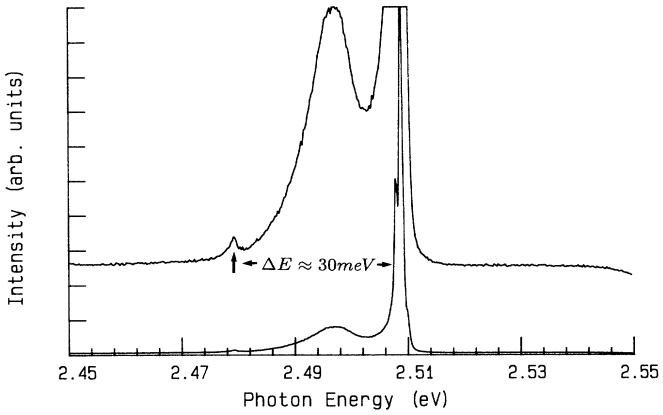

FIG. 6. Raman-scattering spectra of the 6×90 Å MQW (Zn/Cd)Se/ZnSe QW sample at $T=10$ K, with the excitation photon energy around the exciton absorption peak. The narrow peak around 2.51 eV in the figure is the spectrum of the excitation laser. The spectrum has been multiplied by a factor of 10 to highlight the Raman signal (indicated by the arrow).

for the LO-phonon energy in our QW structures. This observation, together with the spectral position of the lasing in Fig. 5, thus also energetically excludes the exciton–LO-phonon scattering mechanism in the stimulated emission process. Furthermore, the large temperature range over which our experiments were carried out (Fig. 1) rules out the possibility of relatively weakly bound excitonic molecules.

We now argue that inhomogeneously broadened excitons should in fact play a principal role in providing gain in the (Zn,Cd)Se/ZnSe quantum wells. Our principal hypothesis begins with the inhomogeneous line shape which defines the initial exciton absorption of the isolated $n=1$ HH resonance at 10 K. Excitons in our quantum-well structures are subject to localization (at low temperatures) and scattering (at higher temperatures) due to the random QW thickness variations and, more importantly, to the alloy compositional fluctuations (note the relatively typical high Cd concentration of 24%). The compositional fluctuations in mixed crystals generally reveal themselves at low temperatures through an inhomogeneously broadened absorption profile with a Gaussian line shape.[20] If a given localization site or a volume defined by the mean free path can only be occupied by one exciton, that is, the exchange interaction between the electrons and holes of different excitons is considered to be infinitely large, the population inversion condition for such excitons is

$$f-(1-f)=2f-1>0\ , \tag{2}$$

where f is the probability of the localized state being occupied. (The validity of this assumption and the isolation of the exciton resonance from the continuum states will be examined below for a higher-temperature situation, where homogeneous broadening by exciton–LO-phonon interaction becomes important.) Under these assumptions, the gain or absorption at a particular photon energy is the sum of the contributions of the exciton states which originate from different localization sites through finite homogeneous broadening. In our terminology, the concept of a localization volume at low temperature becomes an equivalent volume defined by the exciton mean free path at higher temperatures. The contribution to the interband optical response is positive (gain) if the particular site is occupied, and negative (absorption) if it is unoccupied. This is simply a variation of the phase-space filling (PSF) argument,[21] now applied to an inhomogeneously broadened resonance. Of course, we must also assume that the exciton density remains sufficiently low so that the exciton is stable against the formation of an electron-hole plasma. Theory[21,22] and experiment[23,24] on bulk III-V semiconductor and QW's have clearly shown that, when accounting for the many-body Coulomb interactions in a densely populated system, the exciton (interband) energy remains very nearly constant while the free-electron-hole pair states are subject to gap normalization. A transition from an exciton gas to an EHP must occur once the renormalization band gap falls below the exciton energy.

Especially in the case of direct resonant excitation of the HH exciton, the principal physical processes which define the optical response for our (Zn,Cd)Se/ZnSe QW's are (i) exciton energy relaxation to low-energy states of the absorption line through exciton-exciton (no momentum conservation due to the inhomogeneous nature) and exciton-phonon scattering; (ii) PSF of these states; and (iii) homogeneous broadening of the exciton resonance due to the exciton-exciton and exciton-phonon interactions. These processes naturally give rise to the presence of gain on the low-energy tail of the exciton absorption profile, as can be readily described by the phenomenological approach outlined next. In our very simple model, the inhomogeneously broadened exciton resonance effectively forms a multilevel system, where exciton energy relaxation occurs from the initial higher-energy states $|X\rangle$ (relatively delocalized) to the lower-energy states $|X'\rangle$ (relatively localized), from which gain is possible in terms of induced emission to the ground state $|0\rangle$. In broad analogy with the case of a conventional degenerate free electron-hole plasma system, one also needs here a pair density sufficient to drive an initially absorptive material through the transparency condition (absorption saturation) into the gain regime (only in a small spectral region, because of the inhomogeneous nature of the exciton resonance). The gain/absorption coefficient under quasiequilibrium conditions can then be written as the following, if the chemical potential μ is introduced:

$$g(E)=\int_{-\infty}^{+\infty} D_i(E')D_h(E-E')\left[2\frac{1}{e^{(E'-\mu)/kT}+1}-1\right]dE', \tag{3}$$

where D_i is the inhomogeneous and D_h the homogeneous line-shape function. The density of excitons n is given by

$$n=\int_{-\infty}^{+\infty} D_i(E)\frac{1}{e^{(E-\mu)/kT}+1}dE\ . \tag{4}$$

The energies in both equations are defined with respect to

the center of the inhomogeneous exciton resonance. The quantity $g(E)$ is normalized to the peak value of the absorption coefficient, while the exciton density n is normalized to the maximum density of excitons $n_{\max}$ for the total PSF of the inhomogeneous line, a good estimate of which is given by $n_{\max} \approx 1/\pi(a_B^{2D})^2 \approx 5.1 \times 10^{12}$ cm^{-2}. If all the states are empty (corresponding to the situation in an absorption measurement with a weak probe), from Eq. (3) one obtains absorption profiles at different temperatures. The inhomogeneous linewidth in our 6×90-Å QW samples was about 9 meV, in close agreement with that calculated from alloy fluctuations using the approach by Goede, John, and Henning.[25] Rapid energy relaxation on a time scale which is short relative to the stimulated emission events leads to the thermal distribution of the excitons so that the states on the low-energy side of the inhomogeneous line shape become occupied. The homogeneous linewidth convoluted with this distribution then determines the resultant absorption/gain profile. It is illustrative to consider two limits of linewidth broadening. In the limit of extreme inhomogeneous broadening, Eq. (3) evolves to

$$g(E) = D_i(E) \left[2 \frac{1}{e^{(E-\mu)/kT}+1} - 1 \right] . \quad (5)$$

For an exciton resonance with a large oscillator strength (i.e., a large initial absorption) is difficult to achieve gain near the peak of the absorption line for a given exciton density (requiring a large exciton density for absorption saturation of $\alpha \approx 10^5$ cm^{-1}); on the other hand, the necessary threshold gain for laser operation (gain coefficient $g \approx 100$ cm^{-1} is sufficient in our case) is readily available on the low-energy side of the exciton resonance. That is, a moderate amount of partial PSF is adequate to invert an initial absorption $\alpha \approx 100$ cm^{-1} at the low-energy side (a characteristic of an inhomogeneously broadened resonance). In the opposite limit of extreme homogeneous broadening, from Eqs. (3) and (4) we obtain

$$g(E) = D_H(E)(2n-1) . \quad (6)$$

In this case, the entire resonance is either absorptive ($n < 0.5$) or exhibits gain ($n > 0.5$). Now gain is only possible under extreme conditions where the excitonic gas is beginning to lose its stability with respect to the transition to an electron-hole plasma.

The calculated gain/absorption spectra for the 6×90-Å QW structure at 77 and 220 K are shown in Fig. 7, in which the maximum gain coefficient is chosen to be 100 cm^{-1}. The normalized densities of the excitons which produce this gain are $n_s = 0.9 \times 10^{12}$ and 2.5×10^{12} cm^{-2} for the two temperatures, respectively. The values of the initial inhomogeneous linewidth, the peak absorption coefficients, and the homogeneous broadening due to the thermal equilibrium LO-phonon population are taken from the absorption measurement of the particular QW sample on which the experiments were performed. As one limitation of our simple model, we note that the homogeneous broadening $D_H(E)$ should also include the contribution from nonequilibrium LO phonons generated in the exciton relaxation process. A much more fundamental and important limitation, of course, is the neglect of exciton-exciton interactions. Some consequences of this are referred to below in the context of collisional broadening (Secs. V and VI). Nevertheless, the model does highlight the central feature, namely that optical gain can be extracted from the lower-energy side of the exciton resonance. We would also like to note that the distribution function in Eqs. (3) and (4) can take a more general form, especially before the quasiequilibrium condition is reached among the excitons. This will be shown directly in the discussion of the pump-probe measurements in Secs. V and VI.

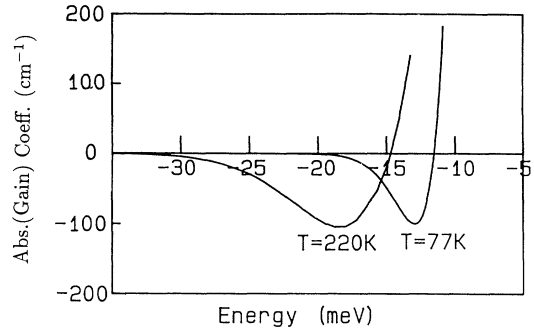

FIG. 7. The relevant portion of the calculated absorption/gain spectrum for the 6×90-Å MQW structure at $T = 77$ and 220 K, according to the phenomenological model described in the text. The horizontal axis indicates the photon energy measured from the center of the $n = 1$ HH inhomogeneously broadened exciton resonance.

Once a sufficient PSF of the states in the low-energy tail of the exciton line is achieved (e.g., $\hbar\omega \approx 2.497$ eV in Fig. 5), the exciton system is in effect inverted at this energy and laser action becomes possible. The energetic relaxation of the exciton population within the states is quite rapid in the (Zn,Cd)Se/ZnSe QW's, as will be shown by the results of the pump-probe measurements in Secs. V and VI.

In contrast to the bulk II-VI semiconductors studied in Refs. 14–19, the large reduction of the exciton–LO-phonon interaction in our QW system keeps the exciton resonance partially inhomogeneously broadened even in the presence a large LO-phonon population. This provides the possibility of having population inversion in only part of the exciton resonance, while the total density of excitons is still low in terms of an exciton-EHP transition density. Of course, given the strong quasi-2D character of our QW system, we also take advantage of the large exciton oscillator strength. As a consequence, in this new circumstance it is unnecessary to demand the exciton-exciton, exciton-electron, or exciton–LO-phonon scattering processes to provide gain, as proposed in the early works on bulk II-VI semiconductors cited above.

V. PICOSECOND PUMP-PROBE EXPERIMENTS AND OTHER SELECTED EXPERIMENTAL OBSERVATIONS

To further investigate the details of excitonic gain and its dynamics, we also performed a set of transient pump-probe experiments on uncleaved QW samples. The ex-

perimental geometry is shown schematically in Fig. 8, where a pair of tunable dye lasers was used to study the details of the $n=1$ exciton resonance under photoexcitation, including the direct quantitative measurement of the gain/absorption and the associated exciton dynamics. To provide the pump and probe source, two Coumarine 480 dye lasers were synchronously pumped simultaneously by a total of 1.2-W ultraviolet laser excitation, obtained by the THG of a cw mode-locked Nd:YAG laser. While the individual laser pulsewidths were approximately 5 ps, the cross-correlation jitter limited the time resolution of the system to about 20 ps. In these experiments, the pump photon energy was directly varied across the exciton resonance, while the fractional changes in the probe beam transmission, the quantity $\Delta T(t)/T$, were measured spectroscopically as a function of the probe pulse delay through the QW in the z direction, following an initial excitation (by the pump pulse) at time $t=0$. More explicitly, we define the differential photomodulated transmission $\Delta T/T \approx -\delta\alpha \times l$ (where l is the effective optical thickness of the QW) as being equal to the difference between transmission of the probe pulses with and without the pump pulses present (normalized to the probe transmission in the unexcited sample), in the small-signal regime. In general, a positive signal in $\Delta T/T$ at a given spectral position can imply real optical gain or induced transparency (decreased absorption), while a negative value of $\Delta T/T$ corresponds to induced absorption. The former results from an electronic (excitonic) occupancy of the states being probed and the latter can originate from pump-induced homogeneous broadening, e.g., due to exciton-exciton collisions or exciton-nonequilibrium–LO-phonon interaction. The signals observed in the experiment are a superposition of these two competing factors (one may dominate the other depending on the particular situation). From an accurate knowledge of the absorption coefficient, our experiments could unambiguously determine whether a positive value of $\Delta T/T$ at a given probe spectral position was indicative of real gain (population inversion) or merely enhanced transparency (partial saturation of absorption but no population inversion).

We now demonstrate the transient characterization of the photoexcited exciton resonance by showing four sets of pump-probe data, each with different choices of pump and probe photon energies. We have chosen the measurement temperature $T=10$ K in order to highlight the exciton dynamics in the extreme inhomogeneous limit. The uppermost trace of Fig. 9 again shows the $N=1$ HH exciton absorption line for spectral reference, as well as the particular choice of photon energy of the pump ($\hbar\omega_{\rm exc}=2.511$ eV, here at the peak of absorption) and three choices for probe photon energy in one such experiment (indicated by smaller arrows). The bottom panels show the transient differential probe transmission for these probe photon energies. The excitation level for all the traces corresponds to an incident energy flux of 1.3 μJ/cm^2 in the 5-ps-long pump pulses, a level of excitation which was sufficient to initiate laser emission in corresponding cleaved structures (see, e.g., Fig. 5, where the laser threshold corresponds to an incident energy density of 0.9 μJ/cm^2). For the probe position at $\hbar\omega_{\rm pr}=2.497$ eV (trace A), where $\alpha l=6.4\times10^{-3}$ without excitation, the peak value of $\Delta T/T$ of 8×10^{-3} *unambiguously indicates the presence of real gain.* On the other hand, at $\hbar\omega_{\rm pr}=2.511$ eV (trace B) the measured $\Delta T/T=0.1$ is simply indicative of partially saturated absorption (note the initial absorbance of $\alpha l=0.57$ at this probe wavelength). Given the measured peak absorption coefficient

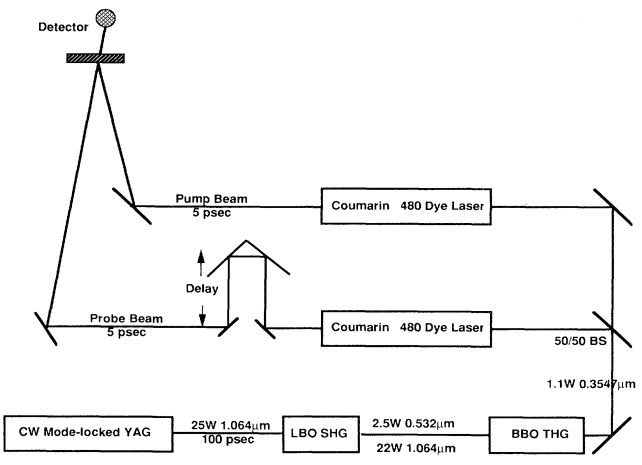

FIG. 8. The schematic diagram of the picosecond pump-probe experiment.

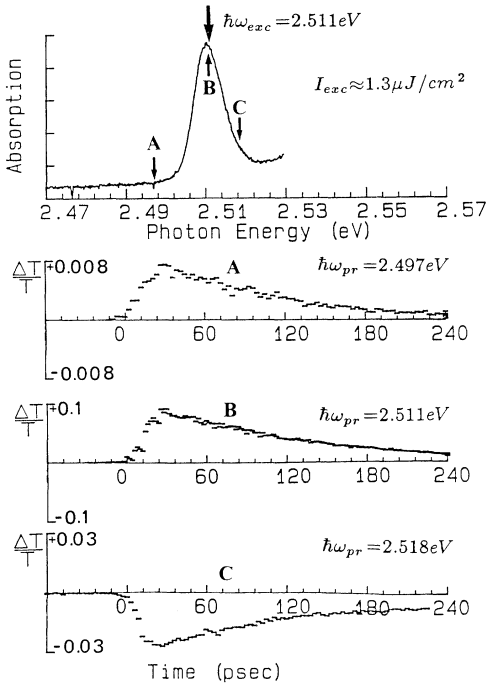

FIG. 9. The transient differential probe transmission $\Delta T(t)/T$ for three different probe energies (labeled A, B, and C) at $T=10$ K, following excitation at $t=0$ by a picosecond pulse at 2.511 eV. The top trace indicates the photon energies relative to the $n=1$ HH exciton resonance of the 6×90 Å MQW structure.

of the unexcited sample of 1.1×10^5 cm^{-1}, the gain coefficient at $\hbar\omega_{pr}=2.497$ eV (in the z direction) can be deduced to be about 60 cm^{-1}. At $T=10$ K and under resonant excitation, the exciton-exciton interaction is the main contribution to the transient homogeneous broadening induced by the pump (collisional broadening). In terms of its magnitude, it is reflected in $\Delta T/T=-3\times10^{-2}$ at $\hbar\omega_{pr}=2.518$ eV (trace C), where the sign reversal indicates the induced absorption.

While exciton energy relaxation and buildup of gain develops on the low-energy side of the resonance, the observed induced absorption is consistent with an effective blueshift of the absorption profile with reduced strength experienced by the probe due to the homogeneous broadening by exciton-exciton interaction which dominates the PSF in these less populated states. This can also be predicted quite readily from the gain expression through a contribution in the change of term $D_h(E)$ in Eq. (3) in Sec. IV, and will be discussed in detail in the next section. Our measurements indicate that the relaxation of the exciton population within the inhomogeneous line is quite rapid in the (Zn,Cd)Se/ZnSe QW system, and close to the resolution of the approximately 20-ps cross-correlation temporal jitter of the dye lasers in our experiments (the rise times in Fig. 9). The typical decay time associated with the traces in Fig. 9 is approximately 200 ps which we verified as being typical of spontaneous exciton recombination times in separate time-resolved photoluminescence studies. To summarize this portion of our pump-probe experimental work, these measurements provide us with direct evidence that under resonant excitation conditions at which lasing occurs in cleaved structure, the system develops optical gain on the lower-energy side of the exciton resonance, which remains well defined at the moderate electron-hole pair density.

Apart from demonstrating the presence of gain, the time-resolved pump-probe experiments also show how the PSF and exciton-exciton interaction (which we consider only in the context of collisional broadening) or exciton–LO-phonon interaction compete with each other while the exciton population is dynamically relaxing and recombining within the inhomogeneous line. In Fig. 10, the pump photon energy is tuned to the low-energy side of the exciton absorption peak and the probe position is chosen at higher photon energies. The top two traces (A and B) show $\Delta T(t)/T$ at $\hbar\omega_{pr}=2.509$ eV, obtained for two different levels of excitation, at 1.3 and 0.13 μJ/cm^2, respectively. No gain at this spectral position is observed (due to the initial large absorbance) and further, the enhanced transparency effect (trace A) is replaced by a short initial induced absorption signal (trace B) at the lower excitation level. In trace C, where the probe photon energy is tuned to the high-energy side of the exciton absorption, the induced absorption persist for approximately the entire exciton lifetime, which is interpreted as a consequence of the exciton-exciton interaction. In traces A and B, because the pump photon energy (at 2.505 eV) is lower than that of the probe (2.509 eV), a competition between the PSF effects and the homogeneous broadening due to the exciton-exciton interaction is strikingly demonstrable as we vary the excitation level.

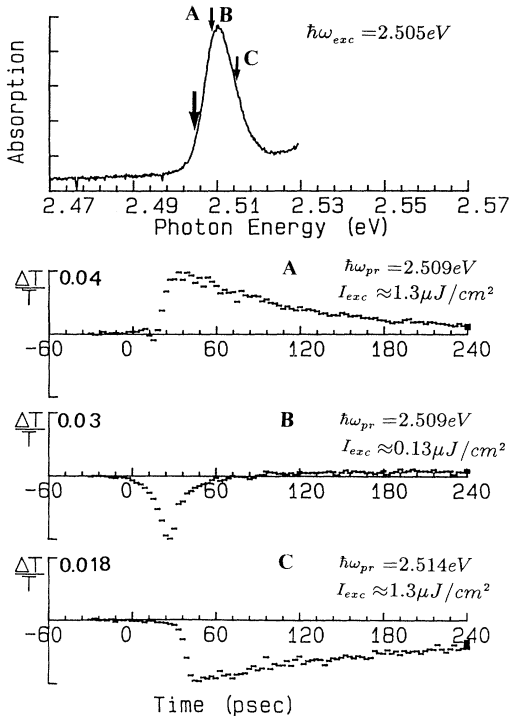

FIG. 10. The transient differential transmission at two different probe energies (labeled A, B, and C) at $T=10$ K, with the pump photon energy 2.505 eV. The $n=1$ HH exciton absorption spectrum of the 6×90-Å MQW sample at this temperature is also shown as a reference. The excitation intensities are also included in the figure.

When the excitation level is low, the PSF aspect is weak and the optical response is initially dominated by the contribution of the collisional broadening to the photomodulated exciton absorption profile, as evidenced in trace B of Fig. 10. On the other hand, the PSF effect becomes the dominant feature at the higher excitation levels, as in trace A.

In Fig. 11, we moved the pump photon energy to the high-energy side of the absorption profile ($\hbar\omega_{exc}=2.515$ eV) in our transient measurement. Here, in the spectral region above the exciton absorption peak, one observes induced absorption as seen in the bottom trace (C) because the exciton-exciton interaction dominates over the PSF contribution to this probe position. On the other hand, at energies in the interval between the pump and the peak of the exciton absorption, the probe ($\hbar\omega_{pr}=2.514$ eV) experiences a relatively short-lived (60-ps) reduction in absorption which can be interpreted as the PSF of these states during the exciton energy relaxation past the probe position, following which the homogeneous broadening due to the exciton-exciton interaction again dominates (the induced absorption in trace B). In trace A, the 2.507-eV probe photons simply sample a dominating PSF effect and therefore experience an induced transparency at this particular level of excitation. As yet another choice of pump photon energy, Fig. 12 shows the transient modulated transmission when the excitation is close to the $n=1$ HH electron-hole continu-

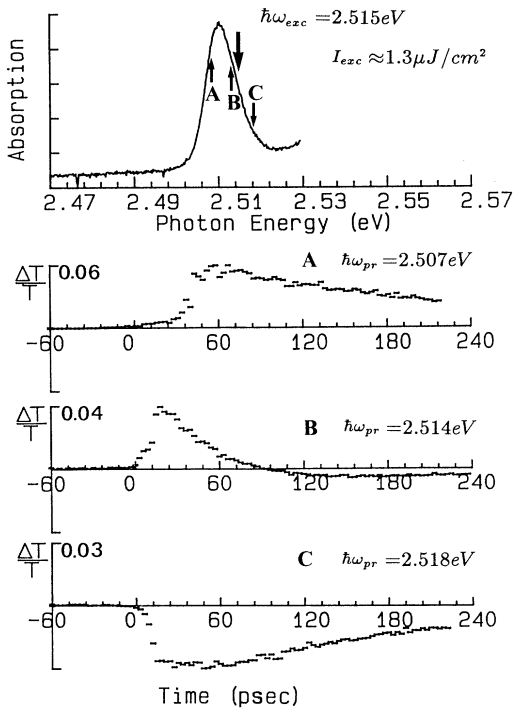

FIG. 11. The transient differential transmission at three different probe energies (labeled *A*, *B*, and *C*) following a picosecond pump pulse with a photon energy of 2.515 eV (on the high-energy side of the $n=1$ HH exciton absorption peak of the 6×90-Å MQW structure) at $T=10$ K.

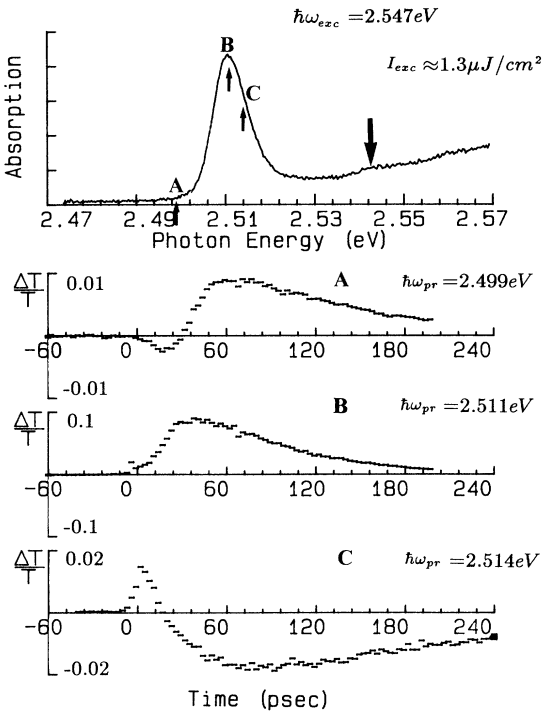

FIG. 12. The transient differential transmission at $T=10$ K for three different probe energies (labeled *A*, *B*, and *C*), with a pump photon energy of 2.547 eV, close to the $n=1$ HH exciton continuum states of the 6×90-Å MQW structure.

um. Again, we find reduced absorption when the probe is situated at the low-energy side of the exciton absorption peak (traces *A* and *B*) and induced absorption on the higher-energy side of the peak (trace *C*) after the excitons reached equilibrium within themselves. However, we also observe the particular initial transients in traces *A* and *C* which reflect the interacting exciton gas during phase-space filling and energy relaxation processes. The special situation here is that at the low-energy side of the absorption peak ($\hbar\omega_{pr}=2.499$ eV, trace *A*), an initial transient induced absorption now due to the exciton collisional broadening and possible exciton nonequilibrium LO-phonon (emitted in the exciton relaxation process) interaction was observed prior to the appearance of gain due to the PSF effects.

Several other experimental observations can be explained using the excitonic gain model outlined in Sec. III. The "Stokes" shift between the photon energy of the laser emission and the $n=1$ HH exciton absorption peak increases somewhat with temperature up to 220 K, as can be measured from Fig. 1. We view this simply as due to the contribution of increased homogeneous broadening, which causes the gain to be extended further away from the center of the overall exciton resonance (as indicated in Fig. 7). However, it is difficult to compare the calculation with the experimental results since we have not taken into account the additional homogeneous broadening due to the exciton-exciton interaction in the calculation. A close comparison between the lasing wavelengths at 10 K in Figs. 1 and 5 shows that under resonant pumping conditions (Fig. 5) the Stokes shift is actually smaller than when the excitation photon energy is near the ZnSe barrier layer band gap. Given our experimental conditions, we can exclude possible lattice heating effects and conclude that in the latter case the nonequilibrium LO-phonon population produced during the exciton relaxation process gives a higher effective exciton temperature in terms of the homogeneous broadening. This aspect is also observed in the excite-probe measurement shown in trace *A* of Fig. 12.

Beyond the temperature of approximately 220 K, homogeneous broadening due to the LO-phonon–exciton interaction in the (Zn,Cd)Se/ZnSe QW becomes an increasingly important factor. The density of the excitons required to achieve optical gain is higher and higher. In the context of our statistical treatment of excitons in the gain model of Eqs. (2) and (3), this implies that the exchange interaction between the excitons in different portions of the inhomogeneous line has to be taken into account. In addition, even with the large exciton binding energy $E_x\approx 40$ meV, finite overlap of the states between the $n=1$ HH excitons and the corresponding free-particle continuum (due to the homogeneous broadening) now becomes a factor. When thermal distribution effects are added into consideration (including 1*s* and all other states), this means that we can no longer treat the 1*s* resonance as being isolated. This can be seen in Fig. 13, where we show the emission spectra of the edge emitting QW lasers at $T=300$ K with different cavity lengths under the same excitations. Substantial spectral shifts are observed for the cavity length ranging from 60 μm to 1

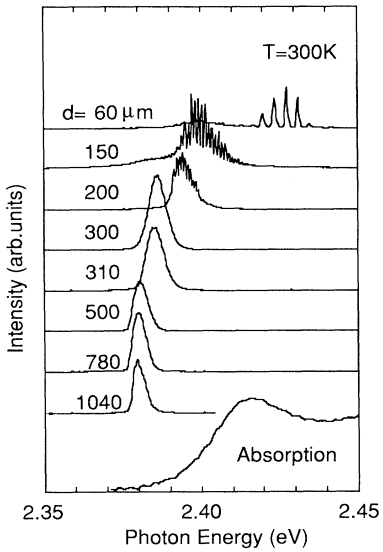

FIG. 13. Lasing spectra at $T=300$ K from 6×90-Å MQW lasers of different cavity length (values are indicated on the figure) under photoexcitations of constant intensity, with the photon energy above the ZnSe band gap. The bottom trace shows the absorption spectrum as a spectral reference.

mm. The spectral position of laser emission is determined by the maximum net gain position, including the cavity loss (dominated by the resonator end facet reflection). A shorter cavity laser therefore has a higher threshold gain coefficient and a higher required density of excitons, a situation which also feeds back to a further contribution to homogeneous broadening. In strong contrast, when the temperature is lowered (e.g., at $T=77$ K), we find that the laser emission varies only about 1–2 meV for the same group of devices, as expected from our model of the gain mechanism for an isolated inhomogeneously broadened exciton system.

Apart from the cavity length dependence, our observation that the "Stokes" shift of the laser emission decreases somewhat as we approach room temperature (Fig. 1) also indicates the effects of homogeneous broadening in the particular laser device ($T=220$–300 K). Nevertheless, the underlying inhomogeneous aspects of the exciton resonance remains important.

VI. DYNAMICS OF EXCITON GAIN AND LASER EMISSION

The pump-probe measurement presented in the previous section using two picosecond lasers has the advantage of allowing us to inject a monochromatic exciton gas into the system. The variation of the individual excitation photon energy gives us clear pictures of energy relaxation processes of the interacting excitons. However, due to the pulse width limit and the temporal jitter between two synchronously pumped dye lasers, the resolution of the fast exciton relaxation processes and the formation of the gain at the lower-energy side of the exciton resonance is limited to 20 ps. For the same reason, it is hard to describe quantitatively the full absorption/gain spectrum at the $n=1$ HH exciton resonance at a given moment after the arrival of the pump pulse. To obtain such information, we have also performed time-resolved femtosecond pump-probe experiments. The experiments were carried out on the 6×30-Å (Zn,Cd)Se/ZnSe multiple-quantum-well structure at $T=10$ and 77 K to further elucidate the distinctly excitonic origin in the optical gain and its dynamics of formation. The dynamical processes, as discussed in Sec. IV, involve PSF, collisional broadening (in a simplified representation of many-body interaction), and energy relaxation within an inhomogeneously broadened quasi-two-dimensional exciton gas. Both the pump and the probe were derived from the same mode-locked Ti:sapphire laser, whose output was first directed into a frequency-doubling crystal to generate blue-green pulses of 300 fs in duration with a spectral bandwidth of approximately 23 meV. The experiments were carried out under resonant excitation at the $n=1$ HH exciton absorption; the pump-probe experiments were done at excitation levels which were sufficient to initiate the laser emission in corresponding cleaved laser structures. Figure 14 shows the spectral relationship between the $n=1$ HH exciton absorption, the pump spectrum, and the spectrum from the edge-emitting laser at $T=77$ K, with well-defined longitudinal modes ($l_c\approx150$ μm). The absorption spectrum has an inhomogeneous width of approximately 15 meV, again dominated by alloy concentration (potential) fluctuations[25] and a small contribution by well-thickness variations. Our experimental conditions are accurately calibrated so that the initial exciton density created by the femtosecond pump pulse in the figure is $n=5.8\times10^{11}$ cm^{-2}, or $n=0.11n_{\max}$, where the saturation density of excitons, $n_{\max}=1/\pi(a_B^{2D})^2$, corresponds to total phase-space occupancy. The QW sample was optically thin so that only 14% of the total incident radiation power was absorbed. Compared to the picosecond pump-probe scheme, we obtain better time resolution (about 300 fs); moreover, the spectral bandwidth of the probe can be used to study the change of the absorption/gain within the entire relevant spectral range around the $n=1$ HH exciton resonance. On the other hand, the use of a femtosecond laser source leads to an initial exciton population (at $t=0$) of a finite bandwidth, determined by the overlap of the laser and the $n=1$ HH

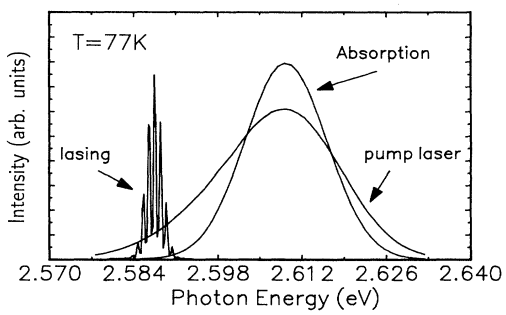

FIG. 14. The absorption spectrum near the $n=1$ HH exciton resonance of the 6×30-Å (Zn,Cd)Se/ZnSe MQW, the pump laser spectrum, and the laser emission from a QW structure at $T=77$ K, respectively.

exciton absorption spectra. Note that the situation in Fig. 14 corresponds distinctly to the case where $n < n_{max}$.

Figure 15 shows the differential transmission $\Delta T/T$ of the probe at early times relative to the resonant photoexcitation at $T = 10$ and 77 K. The excitation level was chosen to be the same as in the corresponding edge-emitting laser studied separately. The figure shows three differential spectra at time delays of -300, 0, and $+300$ fs relative to the arrival of the peak in the pump pulse at the sample. The arrows in the figure indicate the peak in the $n = 1$ HH exciton absorption. Reduced absorption around the center of the exciton resonance occurs immediately with the arrival of the pump, while induced (additional) absorption is present at the wings of the resonance. It is important to note that the exciton absorption peak is not bleached (saturated) even at this initial stage following photoexcitation, consistent with $n < n_{max}$. Qualitatively, the reduction in absorption shows the occupancy of states as well as the broadening by resonantly generated excitons chiefly near the center of the inhomogeneous resonance, while the induced absorption effects reflect this additional homogeneous broadening due to the presence of the interacting exciton population. Examination of Fig. 15 shows little difference in the transient spectra between $T = 10$ and 77 K; in both cases, evidence for incipient exciton energy relaxation is seen at $\tau = 300$ fs in the form of the small redshift of the peak at $\Delta T/T$.

With increasing time delay, one can see direct evidence of the evolving contributions by exciton population redistribution and the homogeneous broadening components. Figure 16 shows the differential probe transmission spectra at time delays of $\tau = 300$ fs, 1.5 ps, and 10 ps at $T = 10$ K and at 300 fs, 900 fs, and 10 ps at $T = 77$ K. While the

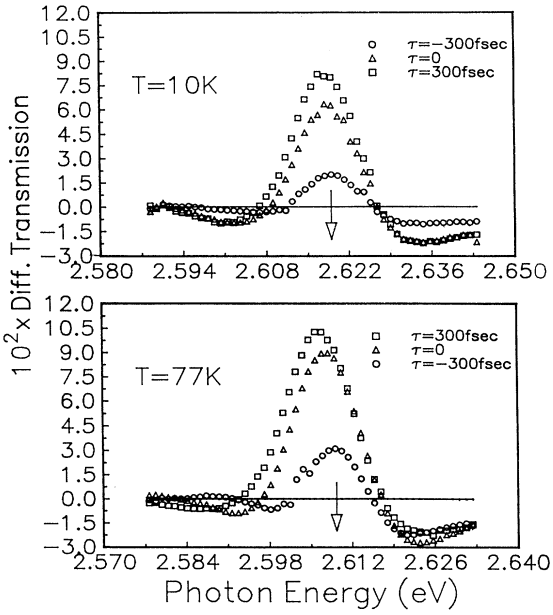

FIG. 15. The differential probe transmission at the $n = 1$ HH exciton resonance on a subpicosecond time scale at $T = 10$ and 77 K. The peak of the $n = 1$ HH exciton absorption is indicated by the arrow.

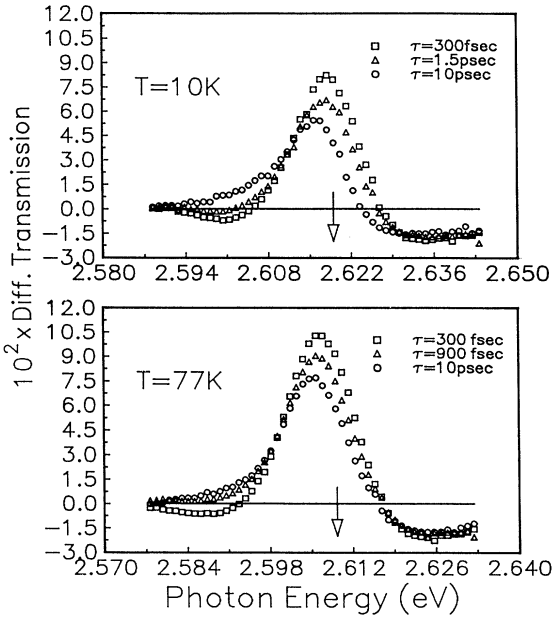

FIG. 16. The differential probe transmission on a picosecond time scale showing the formation of gain on the low-energy portion of the exciton resonance at $T = 10$ and 77 K. The three spectra correspond to the indicated time delays. The peak of the exciton $n = 1$ HH absorption is indicated by the arrow.

negative (i.e., induced absorption) signal is maintained on the high-energy side of the exciton peak, it clearly reverses sign on the low-energy side. This change reflects the filling of exciton states in the tail of the inhomogeneous resonance by the population relaxation effects. The relaxation is rather rapid, with the sign change in $\Delta T/T$ occurring in about 1.5 ps at $T = 10$ K and 0.9 ps at $T = 77$ K, pointing to the role of relatively delocalized excitons in the population redistribution process. Real optical gain reaches a maximum approximately 10 ps fol-

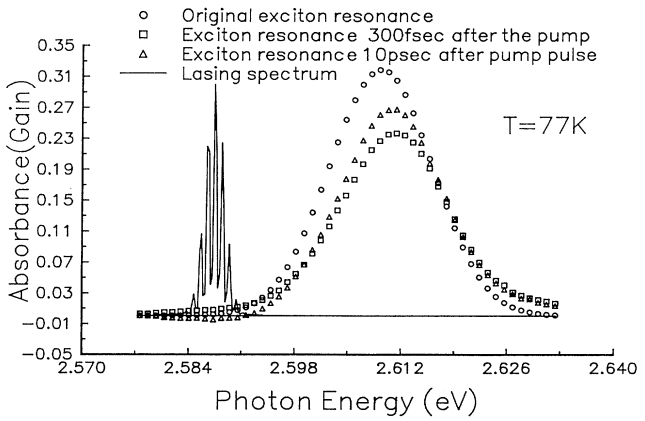

FIG. 17. The $n = 1$ HH exciton absorption resonance at $T = 77$ K without photoexcitation (circles), at 300 fs (squares) and 10 ps (triangles) after the photoexcitation. The QW laser emission spectrum is also included.

lowing the excitation; this can be unambiguously determined from the measured $\Delta T/T$, given the known initial absorption coefficient. The actual gain spectrum at $T=77$ K peaks at approximately $\hbar\omega=2.587$ eV, in good agreement with the lasing spectrum obtained from cleaved samples, pumped at comparable excitation levels.

The presence of gain on the one hand, and the preservation of the exciton resonance on the other, is clearly demonstrated in Fig. 17, where the $n=1$ HH absorption/gain spectra at $T=77$ K are shown at $\tau=300$ fs and 10 ps following the excitation. The data are obtained directly from Figs. 15 and 16 and the unperturbed exciton absorption spectrum which is shown for reference. The laser emission spectrum is included, consistent with the presence of gain on the lower-energy side of the exciton peak. We wish to underline this result: namely, that gain and stimulated emission is produced while the excitonic resonance itself is still maintained. For example, the actual gain coefficient obtained from the experimental data in Fig. 17 at $T=77$ K is $g\approx 130$ cm^{-1} at $\hbar\omega=2.587$ eV, while the reduction in the absorption coefficient at the peak of the resonance is $\delta\alpha\approx 2\times 10^3$ cm^{-1} (here the optical thickness l is taken to be the total thickness of the QW section). It is also interesting to note that we are able to obtain a gain coefficient which is actually larger than the unperturbed absorption coefficient, owing to the additional homogeneous broadening by the interacting exciton population.

The results can be interpreted quite well using the phenomenological model which treats the $n=1$ exciton absorption as an isolated resonance, as sketched in Sec. IV. Using a more general expression for the exciton distribution function $f(E)$ applicable for the present transient case, the change of the absorption/gain is written as

$$\begin{aligned}\Delta T/T=\delta g(E)l=-\delta\alpha(E)l&=\int_{-\infty}^{+\infty}D_i(E')D_h'(E,E')[2f(E')-1]dE'-\int_{-\infty}^{+\infty}D_i(E')D_h(E,E')(-1)dE'\\&=\int_{-\infty}^{+\infty}D_i(E')D_h'(E,E')2f(E')dE'+\int_{-\infty}^{+\infty}D_i(E')[D_h(E,E')-D_h'(E,E')]dE'\ ,\end{aligned}\tag{7}$$

where D_i is the inhomogeneous line-shape function, and D_h' and D_h are homogeneous line-shape functions with and without the interactions among the excitons. Note that we have compressed all the many-body physics into $D_h'(E)$ in this highly simplified approach. The density of excitons n is given by

$$n=\int_{-\infty}^{+\infty}D_i(E')f(E')dE'\ .\tag{8}$$

The second term of the second line in Eq. (7) merely represents an additional broadening of the exciton resonance, as seen experimentally in Figs. 15 and 16. The first term is related to the effects of phase-space occupancy of the exciton population. At $T=77$ K and in our conditions of photoexcitation, the first term can easily dominate the overall expression in the energy range below the absorption maximum due to the relatively small contribution to the linewidth by $D_h'(E,E')$. This explains qualitatively why gain (and stimulated emission) is possible in a portion of the exciton resonance, while at other portions either reduced absorption or induced absorption is witnessed.

Equations (7) and (8) also satisfy the following "sum rule":

$$\int_{-\infty}^{+\infty}\delta g(E)dE=2n\ .\tag{9}$$

Therefore, the total exciton population can be calculated by using the experimental data represented by Figs. 15 and 16. For example, at a 300-fs delay the exciton density is calculated to be 5×10^{11} cm^{-2} at $T=77$ K, which is in good agreement with estimates of this density from the photoinjection conditions of Fig. 1. The overall $\Delta T/T$ spectra, reflecting the total exciton population, has been measured to decay with a time constant of approximately 200 ps (in the absence of a resonator), consistent with the radiative decay of the quasi-2D excitons obtained in separate time-resolved photoluminescence experiments. We also note that the large instantaneous nonlinear response around the exciton resonance always results in the so-called "coherent artifact" near zero time delays in high-intensity femtosecond pump-probe experiments. In our case, this effect has been observed when the probe delay is less than 600 fs and the spectrally integrated signal strength is estimated to be less than 5% of the total signal detected. This, however, does not affect the conclusions we have obtained about the inhomogeneously broadened excitons providing optical gain as the gain is observed 10 ps after the pump laser. The conclusion that the exciton resonance is affected by the extra homogeneous broadening introduced by the exciton population should also hold, because the same effects are also observed in the picosecond pump-probe experiments where the coherent effects are negligible.

We have also applied time-resolved techniques to study the dynamics of laser emission under the resonant pumping conditions described above. The edge emission in this case was detected by a streak camera with a resolution of 13 ps. To increase the photon lifetime in the resonator, reflective coatings were applied to the end facets (with $R\approx 0.9$). Figure 18 shows the time evolution of the QW laser emission at $T=77$ K (with a spectrum such as that in Fig. 17), under femtosecond resonant excitations at three levels of pumping intensities. Note that the pulse formation depends on the excitation level (with respect to the threshold intensity $I_{\rm th}$) and is time delayed with respect to the excitation in the range from 64 to 32 ps. (The pulses at $t\approx 0$ ps represent scattered pump radiation, thus giving both the timing calibration as well as the system temporal resolution.) A key point is that the laser emission occurs on a time scale following the excitation

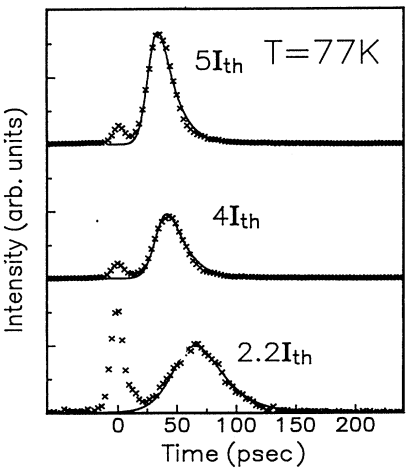

FIG. 18. Temporal profiles of the QW laser emission (crosses) under femtosecond excitation at three different pumping levels (I_{th} is the threshold intensity). The solid lines are a fit to the model described in the text. The peak at $t=0$ is due to scattered pump radiation.

which is consistent with the transient formation of gain shown above. To understand the gain switching and pulse formation kinetics more explicitly, we have applied a simple gain depletion model[26] in which an initial gain appears abruptly at $t=0$, proportional to the excitation intensity. As seen in the figure, a good agreement can be obtained between experiment and the model. Shortest pulses are obtained at the highest level of excitation ($I=5I_{th}$) in Fig. 18 yielding a deconvoluted width of 20 ps and a leading edge of 11 ps.

VII. BRIEF COMMENTARY ON THE CONNECTION TO THE BLUE-GREEN QW DIODE LASERS

With active research efforts ongoing in many laboratories to advance the new blue-green diode lasers based on the (Zn,Cd)Se QW's, a question arises naturally about the conclusions derived in this paper and their relevance to the diode laser case. We note first that the best threshold current densities in the diode laser to date range from about 200 A/cm^2 at $T=77$ K to about 1 kA/cm^2 at room temperature (the latter with high reflectivity end facets).[27] This corresponds to an injected electron-hole pair density of about 10^{11} cm^{-2}, if a radiative decay time of 100 ps is assumed. On the one hand, such a density is low in terms of the exciton-EHP phase transition, and comparable to the densities used in this work. On the other hand, the density is also low in terms of the well-known and necessary inversion condition for a conventional EHP laser, that is, $E_{Fe}-E_{Fp}>\hbar\omega$, where the difference between the electron and hole quasi-Fermi energies must exceed the photon energy. It is therefore conceivable that the aspect of excitonic gain is also an important factor in the diode laser case, even though the method of carrier injection is quite different from the resonantly pumped optical case.

In drawing comparisons between the excitonic and EHP gain mechanisms, we also wish to point out the consequence of the large Fröhlich interaction in the II-VI semiconductors on this issue. The scattering by optical phonons of either excitons or electrons and holes, respectively, leads to a shortening of the momentum (and possible energy) relaxation time. In Sec. IV, we have shown how the homogeneous component from this effect decreases the excitonic gain with increasing temperature. The Fröhlich Hamiltonian for an exciton generally predicts a somewhat smaller scattering cross section than that for an independent electron-hole pair, due to a partial cancellation due to the wave-function overlap in the former case. Even so, as the results of Sec. IV show, the scattering is expected to be a major detrimental factor at room temperature. In terms of the EHP model for gain, the low carrier (hole) mobilities recently measured for p-ZnSe (Ref. 28), suggest that momentum relaxation effect must be taken into account when estimating such gain. The physical effect of the LO-phonon scattering here leads to substantial homogeneous broadening of the density of states, i.e., to the presence of a homogeneously broadened low-energy tail on the order of several tens of meV (even when allowing partial screening of the Fröhlich interaction by the plasma). This aspect may, in fact, give the excitonic gain another advantage over the EHP mechanism.

VIII. SUMMARY AND CONCLUSIONS

In summary, we have presented direct evidence of quasi-2D excitons being responsible for laser emission in the (Zn,Cd)Se/ZnSe quantum-well systems. The inhomogeneous broadening of the exciton resonance provides us with an effective multilevel system, which, coupled with the enhancement in the oscillator strength, makes laser action possible, beginning from the low-energy side where the density of state is very small. This circumstance is connected to the enhancement of the exciton binding energy, which also reduces the homogeneous broadening due to the exciton–LO-phonon coupling with respect to bulk material. The combination of these effects leads directly to lower electron-hole threshold densities for laser action, when compared with the conventional case of a degenerate EHP case, which should also be of practical relevance in the design of blue-green laser diodes.

ACKNOWLEDGMENTS

This research was supported by the Defense Advanced Projects Agency, under the University Research Initiative program (N00014-90-J-1582) and by the National Science Foundation. The authors thank Professor J. Furdyna and co-workers at the University of Notre Dame and Professor R. Gunshor and co-workers at Purdue University for their role in preparing many quantum-well structures.

*On leave from Tohoku University, Sendai, Miyagi, Japan.
[1]M. A. Haase, J. Qiu, J. M. Depuydt, and H. Cheng, Appl. Phys. Lett. **59**, 1272 (1991).
[2]H. Jeon, J. Ding, W. Patterson, A. V. Nurmikko, W. Xie, D. C. Grillo, M. Kobayashi, and R. L. Gunshor, Appl. Phys. Lett. **59**, 3619 (1991).
[3]R. M. Park, M. B. Trofer, C. M. Rouleau, J. M. Depuydt, and M. A. Haase, Appl. Phys. Lett. **57**, 2127 (1990); K. Ohkawa *et al.*, Jpn. J. Appl. Phys. **30**, L152 (1991).
[4]H. Jeon, J. Ding, A. V. Nurmikko, H. Luo, N. Samarth, and J. K. Furdyna, Appl. Phys. Lett. **59**, 1293 (1991); J. Ding, H. Jeon, A. V. Nurmikko, H. Luo, N. Samarth, and J. K. Furdyna, *ibid.* **57**, 2756 (1990); H. Jeon, J. Ding, A. V. Nurmikko, H. Luo, N. Samarth, and J. K. Furdyna, *ibid.* **57**, 2413 (1990).
[5]H. Jeon, J. Ding, A. V. Nurmikko, W. Xie, D. C. Grillo, M. Kobayashi, and R. L. Gunshor; Appl. Phys. Lett. **60**, 2045 (1992); H. Okuyama, T. Miyajima, Y. Morinaga, F. Hiei, M. Ozawa, and K. Akimoto, Electron. Lett. **28**, 1798 (1992).
[6](a) J. Ding, N. Pelekanos, A. V. Nurmikko, H. Luo, N. Samarth, and J. K. Furdyna, Appl. Phys. Lett. **57**, 2885 (1990); (b) N. Pelekanos, J. Ding, M. Hagerott, A. V. Nurmikko, H. Luo, N. Samarth, and J. K. Furdyna, Phys. Rev. B **45**, 6037 (1992).
[7]N. Samarth, H. Luo, J. K. Furdyna, R. G. Alonso, Y. R. Lee, A. K. Ramdas, S. B. Qadri, and N. Otsuka, Appl. Phys. Lett. **58**, 1163 (1990).
[8]W. Walecki, A. V. Nurimikko, N. Samarth, H. Luo, and J. K. Furdyna, J. Opt. Soc. Am. B **8**, 1799 (1991).
[9]E. O. Göbel, in *Excitons in Confined Systems,* edited by R. Del Sole, A. D'Andrea, and A. Lapiccirella, *Proceedings of Physics Vol. 25; Proceedings of the International Meeting, Rome, 1987* (Springer-Verlag, New York, 1988), p. 204.
[10]H. W. Hölscher, A. Nöthe, and Ch. Uihlein, Phys. Rev. B **31**, 2379 (1985).
[11]D. S. Chemla, S. Schmitt-Rink, and D. A. B. Miller, in *Optical Nonlinearity and Instabilities in Semicoductors,* edited by H. Haug (Academic, Boston, 1988), p. 83.
[12]J. Lee, E. Koteles, and M. O. Vassell, Phys. Rev. B **33**, 5512 (1986).
[13]C. van der Walle, Phys. Rev. B **39**, 1871 (1989).
[14]J. M. Hvam, Solid State Commun. **12**, 95 (1973).
[15]S. W. Koch, H. Haug, G. Schmieder, W. Bohnert, and C. Klingshirn, Phys. Status Solidi B **89**, 431 (1978).
[16]K. Bohnert, G. Schmieder, and C. Klingshirn, Phys. Status Solidi B **98**, 175 (1980).
[17]H. Haug and S. W. Koch, Phys. Status Solidi B **82**, 531 (1977).
[18]F. A. Majumder, S. Shevel, V. G. Lyssenko, H. E. Swoboda, and C. Klingshirn, Z. Phys. B **66**, 409 (1987).
[19]P. R. Newbury, K. Shahzad, and D. A. Cammack, Appl. Phys. Lett. **58**, 1065 (1991).
[20]H. Sumi, J. Phys. Soc. Jpn. **32**, 616 (1972).
[21]See, e.g., S. Schmitt-Rink, D. S. Chemla, and D. A. B. Miller, Adv. Phys. **38**, 89 (1989).
[22]R. Zimmerman, K. Kilimann, D. Kremp, and G. Roepke, Phys. Status Solidi B **90**, 175 (1978); R. Zimmerman, *Teubner-Texte zur Physik* (VOB National, Berlin, 1988), Vol. 18, pp. 1–176.
[23]N. Peyghambarian, H. Gibbs, J. Jewell, A. Antonetti, A. Migus, D. Hulin, and A. Mysyrowicz, Phys. Rev. Lett. **53**, 2433 (1984).
[24]G. W. Fehrenbach, W. Schafer, J. Treusch, and R. G. Ulbrich, Phys. Rev. Lett. **49**, 1281 (1982).
[25]O. Goede, L. John, and D. Henning, Phys. Status Solidi B **89**, K183 (1978).
[26]A. Yariv, *Quantum Electronics,* 3rd ed. (Wiley, New York, 1988), p. 534.
[27]J. De Puydt, M. Haase, J. Qiu, and H. Cheng, in *Procedings of the Conference on Blue-Green Lasers, Albuquerque* (Optical Society of America, Washington, DC, 1992); H. Jeon, J. Ding, A. V. Nurmikko, W. Xie, D. C. Grillo, M. Kobayashi, and R. L. Gunshor, *Conference on Lasers and Electro-Optics 1992,* OSA Technical Digest Series Vol. 12 (Optical Society of America, Washington, DC, 1992), pp. 32 and 33; Opt. Lett. (to be published).
[28]Y. Fan, J. Han, L. He, J. Saraie, R. L. Gunshor, M. Hagerott, H. Jeon, A. V. Nurimikko, G. C. Hua, and N. Otsuka, Appl. Phys. Lett. **61**, 3160 (1992).